Multi-jet impingment cooling on a concave surface, under stationary and rotating conditions

MULTI-JET IMPINGMENT COOLING ON A CONCAVE SURFACE, UNDER STATIONARY AND ROTATING CONDITIONS.

Alex Skillen, alex.skillen@googlemail.com
Hector Iacovides, h.iacovides@manchester.ac.uk

Turbulence Mechanics Group, School of Mechanical Aerospace and Civil Engineering, The University of Manchester, M60 1QD, UK

Abstract

This study focuses on the prediction of the flow and thermal development, when cooling fluid form a row of five jets impinges on a heated concave surface of a semi-cylindrical cooling passage. The passage can rotate about an axis normal to it and parallel to the jets. This application is relevant to the internal cooling of the leading edge of turbine blades. The objective is to establish how reliably the flow and thermal characteristics can be predicted, using a commercial CFD package. The FLUENT code is employed for this purpose and three sets of computations have been obtained, one for stationary and two for counter-clockwise rotating conditions. A variant of the k-ε turbulence model is used, with a two-layer near-wall treatment. The jet spacing (jet distance to jet diameter ratio) is 4 and ratio between the radius of the concave surface and the jet diameter is 3.125. The flow Reynolds number, based on the jet velocity and diameter ($Re \equiv V_j d_j / \nu$) is 15,000 and the fluid Prandtl number is 6.09 (water). For the rotating cases examined, the rotation number ($Ro \equiv \Omega d_j / V_j$) is 0.09 and 0.18. The effectiveness of the predictions is assessed through comparisons with local flow and thermal measurements, produced by the authors' group. For the stationary case, the local flow development within the passage and also the local Nusselt number over the concave surface are well reproduced. The heat transfer comparisons for the rotating cases do not show the same degree of agreement between predictions and measurements.

INTRODUCTION

The efficient cooling of blades within a gas turbine is of crucial importance. To achieve efficient cooling of blades within a modern gas turbine, internal blade cooling passages are typically employed. The complex geometrical shape of these passages results in many flow features being present, including separation, reattachment, strong secondary flows and impingement, in addition to system rotation. Some of these features, such as the effects of sharp U-turns and the use of rib-roughness, have received considerable attention in numerous studies. The interested reader is referred to the textbook of Han et al (2000) and the recent review paper of Iacovides and Launder (2007). For other, equally important, features, like impingement cooling the available studies are far fewer and tend to focus on stationary conditions Son et al (2001), Akella and Han (1998) and Parsons and Han (1998) are some such examples. The only study to present local Nusselt number data for impingement on a concave surface under rotating conditions was the mass transfer investigation of Mattern and Hennecke, though this was confined to relatively low rotation numbers and did not include accompanying velocity field data. The present contribution focuses on the prediction of jet impingement onto a concave surface: a situation typically employed for the internal cooling of the leading edge of a blade (see Fig. 1(a)).

At the 8th UK National Heat Transfer Conference, Iacovides et al (2003) and subsequently Iacovides et al (2005), reported detailed flow and heat transfer measurements of a situation relevant to the above application, employing a row of five circular jets impinging onto the concave surface of a semi-circular passage (see Fig 1(b)). Under non-rotating conditions, flow visualisation images and velocity traverses show that the cores of the five jets remain it tact up to the point of impact (which is consistent with the distance from discharge to the impingement surface of only just over three jet diameters) and the resultant radial wall jets collide, giving rise to a noticeable, though, jet ''fountain.'' In the corresponding heat transfer measurements, the imprint of the five jets was clearly visible. Weak secondary peaks in Nu are evident midway between the jet-impingement zones. These arise from the collision of the radially outward wall jets following the jet impingement. Rotation led to the disappearance of the secondary peaks in Nusselt number and the change in the shape of the high Nu contours above each injection hole, from elliptical (with the major axis normal to that of the cooling passage) to more circular. More surprisingly, at the higher rotation rates one of the three inner jets, the central one for clockwise and one of the other two jets for counter-clockwise rotation, produced substantially lower Nusselt number levels. The flow data suggested that rotation generates swirl within the jets, which in turn increases their spreading rates and causes flow instabilities as the jets overlap. It is consequently clear that leading edge impingement cooling involves three-dimensional and highly complex flow structures. Rotation, at levels typical of engine conditions, can lead to unexpected and undesirable thermal features, since low Nusselt number regions will cause local hot spots. The optimisation and indeed further understanding of this process, will be greatly assisted by the availability of robust numerical flow solvers, that can produce reliable simulations of the heat and fluid flow processes involved in the impingement cooling of rotating passages.

Work is in progress within the authors' group, aiming to produce computationally efficient and reliable methods for the prediction of rotating impingement cooling, using our in-house CFD software. Preliminary results have been reported elsewhere, Craft et al (2007). Here the intention is to report attempts to assess the effectiveness of a commercial CFD package, FLUENT, for such applications.

CASES EXAMINED

The experimental geometry is shown in Figure 1(b). It comprises a transparent chamber, semi-circular in cross section beneath which is a horizontal plate with five holes each 11.2 mm in diameter, d_J, and spaced 44.8 mm, s, apart, resulting in a spacing s/d_J of 4. Cooling fluid (water) flows through the holes forming circular jets, which, for zero rotation, impinge symmetrically on the semi-circular surface of radius, R, 35 mm and length, L, of 294 mm. leading to L/d_J of. 26.25. The distance between the jets exit and the target surface is thus 3.124 jet
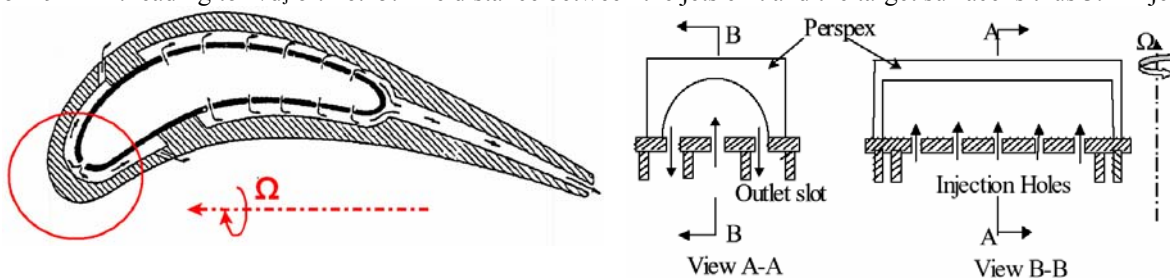
a) Leading edge impingement in a turbine blade   b) Experimental model, Iacovides et al. (2005)

Figure 1: Impingement cooling systems.

diameters. The jet fluid leaves the semi-circular cavity from two slots on the horizontal plane, that, as also shown in Figure 1(b), are symmetrically located on either side of the row of jets. The slot width is 6 mm, or 0.54 jet diameters, the slot length is 270 mm or 24.1 jet diameters and the distance of the centreline of each slot from the centreline of the passage is 32 mm, or 2.9 jet diameters. The top, semi-circular surface of the passage is heated under constant wall heat flux boundary conditions, and all other surfaces are thermally insulated.

Non-dimensionalisation of the flow and enthalpy equations produces the following four relevant independent dimensionless groups.

Flow Reynolds number	Flow Rotation number	Fluid Prandtl number	Flow Rotational Rayleigh number
$\mathrm{Re} \equiv \rho V_J d_J / \mu$	$\mathrm{Ro} \equiv \Omega d_J / V_j$	$\mathrm{Pr} \equiv \nu/\alpha$	$\mathrm{Ra} \equiv \Omega^2 X d_J{}^3 \mathrm{Pr}\beta\Delta\Theta/\nu^2$

In the above expressions U_J is the jet velocity, Ω the angular speed of rotation X the distance from the axis of rotation, $\Delta\Theta$ a characteristic temperature difference, normally the difference between the wall and jet inlet temperatures and ρ, α, μ, ν and β the fluid density, specific heat capacity, thermal diffusivity, dynamic viscosity, kinematic viscosity and coefficient of thermal expansion respectively.

Because in the experimental study of Iacovides et al (2003, 2005), the results of which are used to validate these computations, the value of Ra was low enough (due to low H and $\Delta\Theta$) for rotational buoyancy effects to be negligible, the effects of temperature on the fluid density have been ignored and only the flow Reynolds and rotation number values and the fluid Prandtl number value have been reproduced in this study. Flow at two Reynolds numbers has been computed, 9,400 and 15,000. The fluid Prandtl number the value is 6.09 in all cases presented here. For the two rotating cases, the rotation number values are 0.09 and 0.18 and the direction of rotation corresponds to the counter-clockwise rotation of the experimental study.

EQUATIONS OF FLUID MOTION

Mean Flow Equations

The starting point of any computational analysis is, of course, the set of equations that result from the laws of mass, momentum and heat transport. For blade-cooling applications, these equations need to be formulated for a rotating frame of reference and averaged in a way consistent with the modelling strategy adopted. For RANS treatments the equations may be presented in the compact Cartesian notation form:

$$Mass\quad Conservation\quad Equation \qquad \frac{\partial}{\partial x_i}\left(\rho\, U_i\right) = 0 \qquad (1)$$

Momentum and Enthalpy Transport Equations

$$\frac{\partial}{\partial x_j}\left(\rho U_j U_i\right) = -\frac{\partial P}{\partial x_i} + \frac{\partial}{\partial x_j}\left[\mu\left(\frac{\partial U_i}{\partial x_j}+\frac{\partial U_j}{\partial x_i}\right) - \rho\overline{u_i u_j}\right] - 2\rho\,\epsilon_{ijp}\Omega_p\,U_j - \rho\left[\Omega_j X_j \Omega_i - \Omega_j X_i \Omega_j\right] \qquad (2)$$

$$\frac{\partial}{\partial x_j}\left(\rho U_j \Theta\right) = \frac{\partial}{\partial x_j}\left(\frac{\mu}{Pr}\frac{\partial\Theta}{\partial x_j} - \rho\overline{u_j\theta}\right) \qquad (3)$$

Turbulence Modelling

Embedded within the above forms of the transport equations are the effective-viscosity and effective diffusivity approximations shown below.

$$\rho\,\overline{u_i u_j} = \frac{2}{3}k\delta_{ij} - \mu_t\left(\frac{\partial U_i}{\partial x_j}+\frac{\partial U_j}{\partial x_i}\right) \qquad (4) \qquad \overline{u_i\theta} = -\frac{\mu_t}{\sigma_\Theta}\frac{\partial\Theta}{\partial x_i} \qquad (5)$$

Equations (4) and (5) above show that the effective-viscosity approximation cannot include the influence of rotation on the turbulence field and consequently suggest that turbulence models based on this approximation are not suitable for the prediction of rotating turbulent flows. Since, however, effective-viscosity models are the most widely used turbulence models, in RANS simulations, especially in industry, it is appropriate, indeed essential, that any validation exercise starts by first focussing on this group of models. Here the variant of the
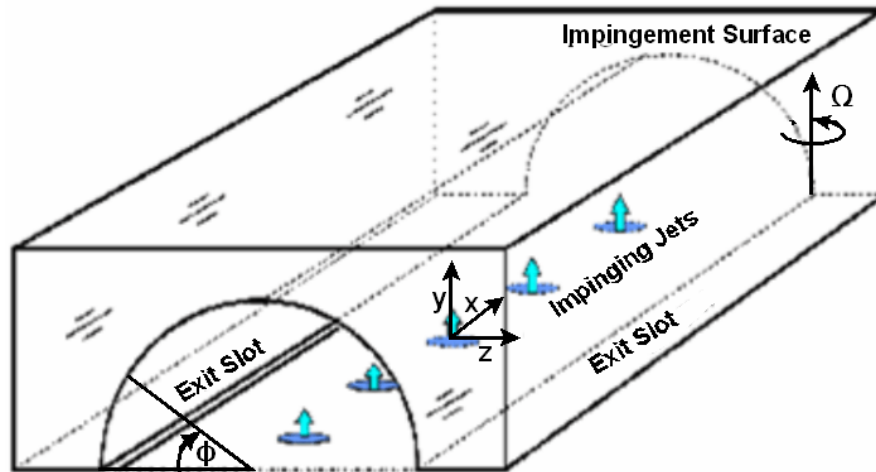
Figure 2. Computational Flow Domain

well known k-ε model available within FLUENT, known as the realisable k-ε, has been used to provide the distribution of the turbulent viscosity, μ_t, which is needed in the approximations of equations (4) and (5). The turbulent Prandtl number, σ_Θ, is assigned the constant value of 0.9.

Since one of the main objectives here is the prediction of wall heat transfer, one issue that requires special consideration, is the modelling of the effects of near-wall turbulence on the transport of momentum and thermal energy across the wall boundary layers. Here the "enhanced wall treatment" option, available within FLUENT, has been employed, which for finer near-wall meshes, switches to a two-layer treatment with a low-Re 1-equation model of turbulence, Wolfstein (1969). Two-layer approaches have long been employed within the authors' group in the computation of complex 3-dimensional flows, Iacovides and Launder (1984, 1987). They provide an often acceptable compromise between predictive accuracy and computational efficiency, since the 1-equation model one the one hand involves less restrictive approximations than log-law-based wall functions and on the other hand is not as expensive as two-equation low-Reynolds-number models.

NUMERICAL ASPECTS

The flow has been specified as steady and incompressible and the second-order upwind scheme has been used for the discretization of convective transport. The computational domain is shown in Figure 2. It matches the experimental geometry shown in Figure 1(b), and all the geometrical parameters have the values given earlier. As in the experimental study, the axis of rotation is located at the top right hand corner of the domain. The computational domain has been reproduced using the multi-block grid shown in Figure 3.

Inlet conditions were identical for the five jets. The mass flow rate was set to the level required to reproduce the experimental Reynolds number. A uniform velocity core was specified over most of the cross section of each inlet pipe, with a turbulent boundary layer, based on the one seventh power law, across the outer 40% of the pipe radius. The inlet turbulence intensity was set the rather high level of 15%. These inlet conditions were in close accord with those measured. The outlet was modelled using the 'outflow' boundary condition. In this condition, FLUENT extrapolates pressure and velocity data from the interior. This was a suitable boundary
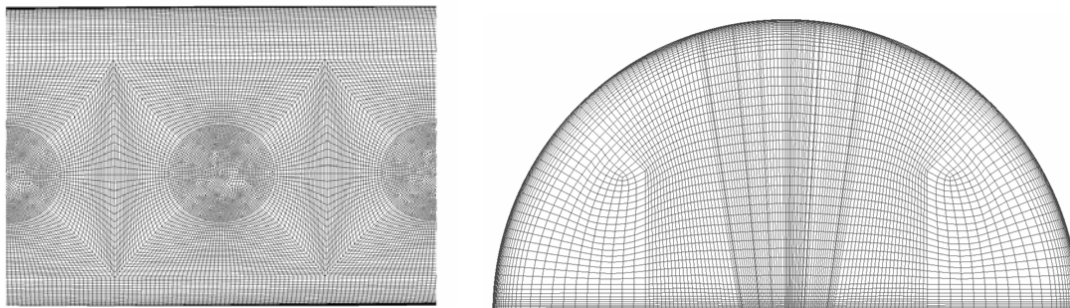
a) Plan view above the central jet.   b) Cross section through central jet
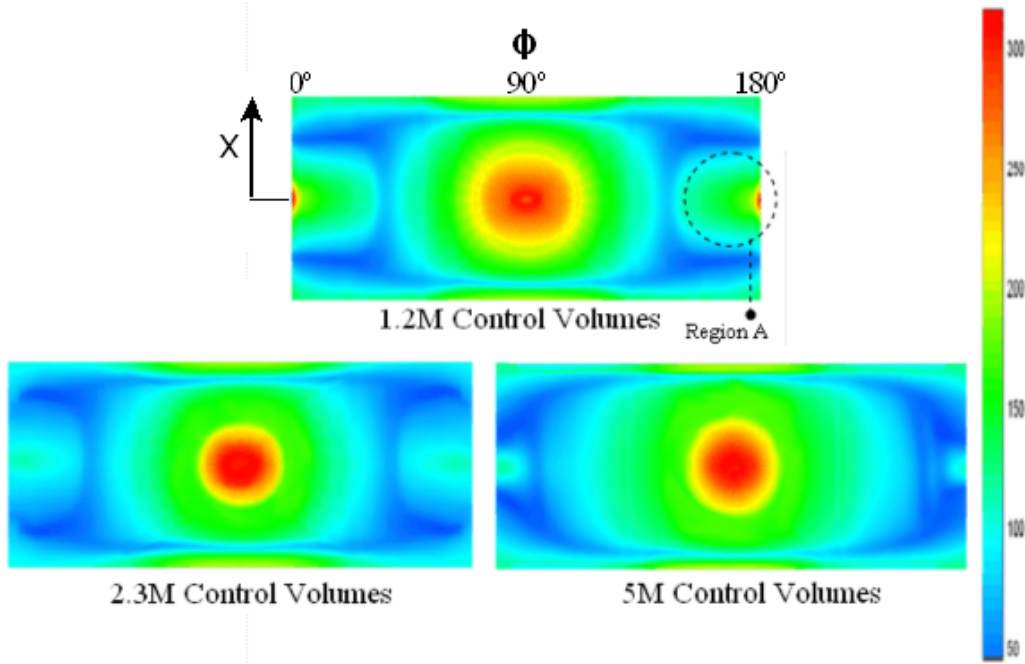**Figure 3**. Grid Generation

4

Figure 4. Grid comparison tests illustrating the Nusselt number variation above the central jet. Ro=0, Re=15,000 and Pr = 6.09

condition since the details of the pressure distribution at the outlet were unknown prior to the solution of the problem. In the experiment the flow did not expel into the atmosphere but into a water tank, hence the pressure distribution is unknown. As far as the thermal boundary conditions are concerned, a fixed inlet temperature was specified, together with constant wall heat flux over the curved surface and adiabatic conditions over the other walls.

Three different mesh sizes have been tested, in order to establish a mesh size necessary to produce grid independent predictions. The first grid consisted of approximately 1.2 million control volumes, the second grid of approximately 2.3 million and finally a third grid of up to 5 million. The numerical quality of the resulting simulations is assessed though the comparisons of the corresponding predictions of the local Nusselt number, Nu [$\equiv q_w.d_J/\{k(\Theta_W-\Theta_J)\}$], variation over the central jet, under stationary conditions, shown in Figure 4. It can be seen that with 1.2 million cells, there is a large over-prediction in Nusselt number at region A. Also, the Nusselt number distribution is fairly different from that of the 2.3 million cell mesh. On the other hand, comparisons between the 2.3 million cell mesh and the 5 million cell mesh show fairly similar results. The 2.3 million cell resolution was therefore used for all subsequent simulations. The near wall nodes were placed at a non-dimensional distance from the wall of $y^+ \leq 4$. Most near wall nodes were found at approximately $y^+ = 1$.

RESULTS

Stationary Case

The assessment of the computations, starts with comparisons between the computed and measured mean flow fields in the cross-sectional plane above the central jet, presented in Figure 5. These suggest that the mean flow development is correctly predicted. In common with the experiments, the present computations show tha the jet core remains in tact until it reaches the close proximity of the target surface and there is very little downward motion. The latter is indicative of the highly three-dimensional character of the flow, with the apparent mass deficit within the cross-sectional planes above each jet, balanced by flow movement in the axial (x) direction. This is indeed confirmed by the comparisons of the flow development within the axial symmetry plane, for the three central jets, included in Figure 6. The development of the cores of the three central jets and also the presence of the formation of a strong fountain between neighbouring jets, which follows from the collision of wall jets that develop from adjacent impingement points, are also well reproduced by the computations. It is thus established, that qualitatively, the current predictions are able to reproduce the development of the jets, along both the cross-duct and the axial directions. The velocity profile comparisons of Figure 7, provide a quantitative assessment of the mean flow predictions. The close agreement between
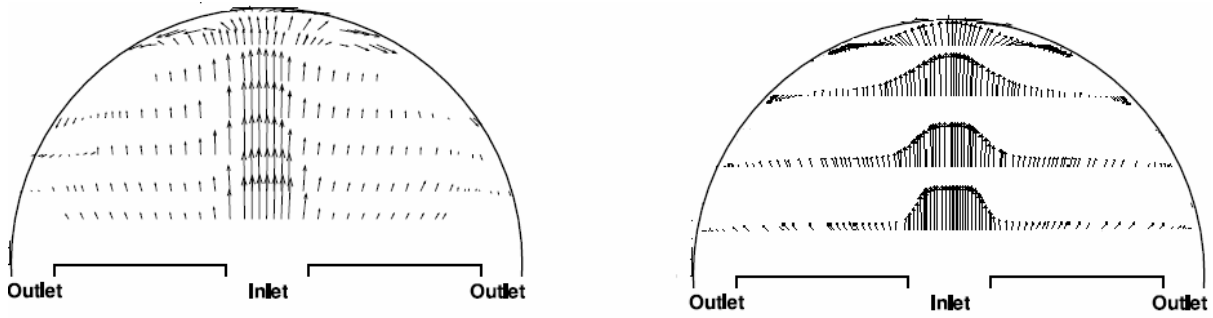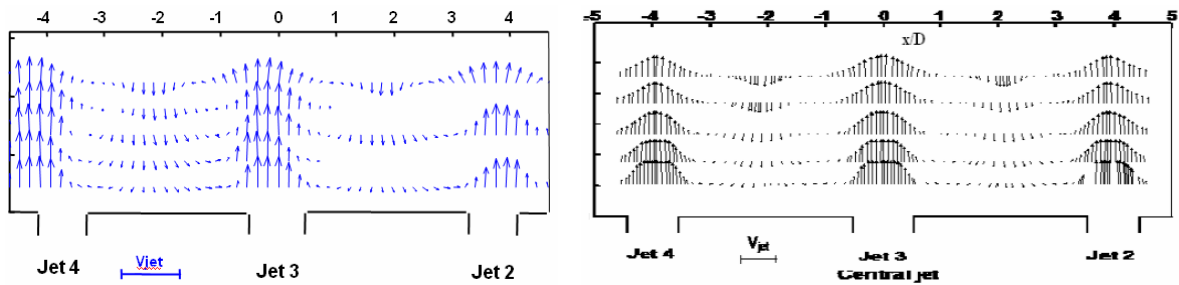
Figure 5. Velocity field comparisons for cross-sectional plane above central jet, for stationary case. Experiment, Iacovides et al (2005), left and computation right. Re= 9,400.


a) Measurements, Iacovides et al (2005)   b) Present Computations
Figure 6. Velocity field comparisons axial symmetry plane above the three central jets, for stationary case. Re= 9,400.

predictions and measurements along the traverse line closer to the jet exit (y/d_J=0.55) confirms that appropriate entry conditions have been specified. What is more encouraging, is that at about half way between the jet exit and the top surface (y/d_J=1.34), the jet development is well reproduced by the computations though the downward velocity near the walls is not reproduced. Closer to the top wall (y/d_J=2.86), the jet centreline velocity is under-predicted somewhat, suggesting that the predictions under-estimate the spreading rate of the jet, though obviously not within the cross sectional plane y-z. Overall, the mean flow comparisons of Figures 5, 6 and 7 suggest that the jet development is well predicted.

The profiles of the vertical component of the turbulence intensity, shown in Figure 8, provide the opportunity to assess how well the turbulence field is computed, which in turn may explain some of the predictive deficiencies identified in the mean flow comparisons. It is evident that, as the jet develops, the turbulence intensity is generally underestimated. This must be, in part at least, due to the underlying assumptions of the k-ε turbulence effective viscosity model, which fails to take into account the effects of turbulence anisotropy. Another possible cause for the under-estimation of the turbulence levels is that, as suggested by flow visualisation videos that can viewed at http://tmgflows.mace.manchester.ac.uk/,
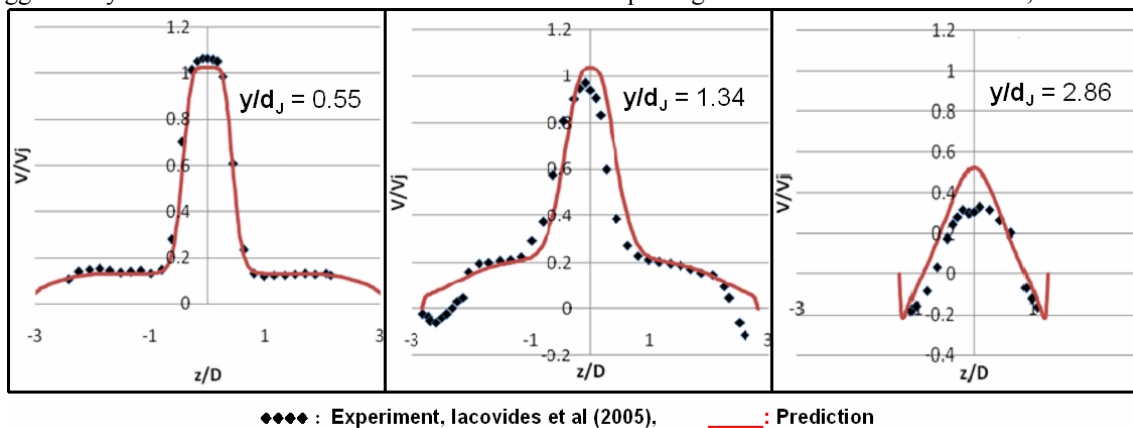
♦♦♦♦ : Experiment, Iacovides et al (2005),   _____ : Prediction

Figure 7. Comparisons of profiles of the vertical velocity component across the passage, over the central jet. Stationary case, Re= 9,400.
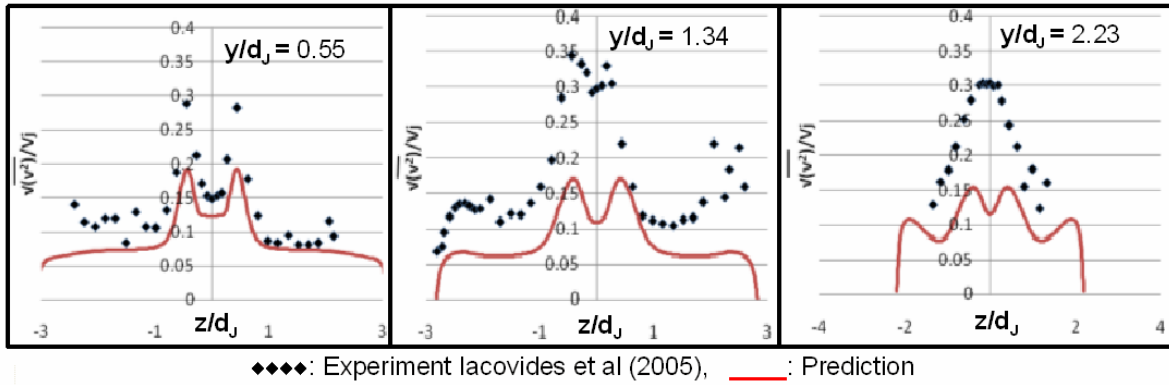
6

Figure 8. Comparisons of profiles of the vertical component of the turbulence intensity across the passage, over the central jet. Stationary case, Re= 9,400.

the flow becomes unstable with some low frequency flapping of the jets. This cannot be captured with the steady state flow computations presented here. The higher turbulence levels measured, are certainly consistent with a stronger entrainment of the ambient fluid surrounding the jet and consequently a jet centreline velocity lower than that predicted, as the jet develops.

The reliability of the heat transfer predictions, is now assessed through the comparison of the contours of the local Nusselt number in Figure 9. It can be seen that both the overall level of the Nusselt number as well as the special variation are well predicted. The peak values of the Nusselt number at the stagnation region above each jet are well reproduced and the formation of secondary peaks in Nu half-way between stagnation points is also captured in the computations. Some, though not major, differences between predictions and measurements can be seen. In the predicted contours, however, the size of the high Nu regions at the stagnation points is not as high as in the measurements. For the central jet, the high Nusselt number region is circular, in contrast to the elliptical shape observed in the measurements. Another deviation from the measured thermal development, is that in the predicted levels of the secondary Nu peaks are lower. The modest under-estimation of the spreading rate of the jets and also the more substantial under-estimation of the jet turbulence levels are certainly compatible with the differences identified in the thermal comparisons. A more likely cause, is the modelling of the near-wall turbulence. The "enhanced wall treatment" used here, for the grid employed, is in effect a 2-layer treatment with an 1-equation near-wall model of turbulence. The 1-equation model, because it determines the length-scale of turbulence from the wall distance, under-predicts near-wall turbulence levels and consequently wall heat flux coefficients. Given the relative simplicity of the effective-viscosity approximation and the treatment of the near-wall turbulence, agreement with the thermal data is satisfactory to a surprising degree.
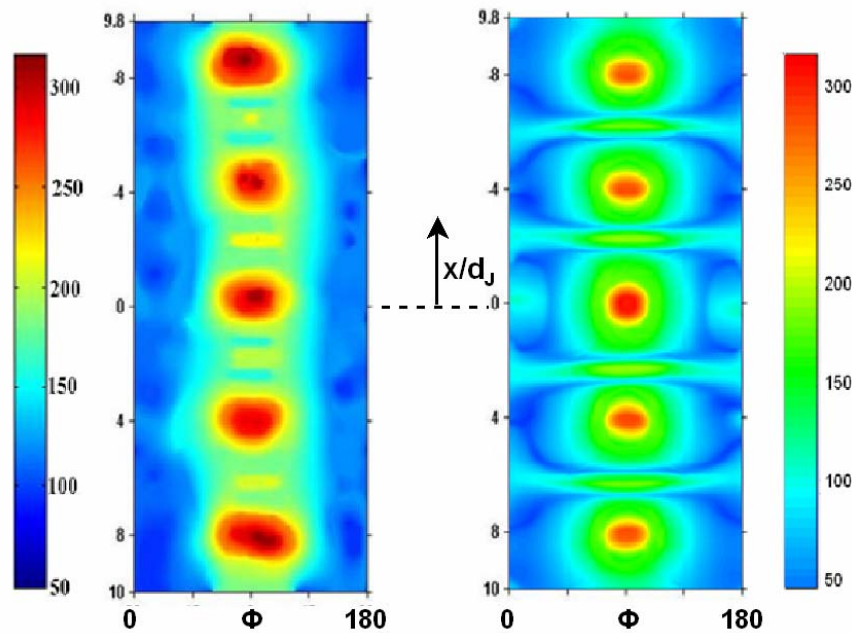
a) Experiment, Iacovides et al (2005)   b) Computation
Figure 9. Nusselt number comparisons for stationary case, Re=15,000 and Pr =6.09.

7

Rotating Cases

The discussion on the rotating flow predictions, starts with the local Nusselt number comparisons, shown in Figure 10. At a rotation number of 0.09, the experimental data, Figure 10a), show that most peak Nu regions above the jets change in shape from elliptical to round, the peak Nu values are reduced, some of the secondary peaks between impingements points disappear and the others diminish and, most strikingly perhaps, the peak Nu region above jet 4 is substantially reduced in size and the peak Nu levels within it are markedly lower in comparison to the corresponding regions above the other jets. In the corresponding computations, shown in Figure 10b), in accord with the data, the shape of the peak Nu regions has changed to round, there is an overall reduction in the Nusselt number levels and the secondary peaks between the stagnation regions are substantially diminished. Moreover the computations indicate that the Nu distribution is now anti-symmetric rather than symmetric across the Φ=90 centreline, due of course to the Coriolis force. What the computations fail to reproduce, is the diminution in the peak levels above jet 4. A doubling of the rotation number, Figure 10c), causes further reduction to the overall Nusselt number levels, the disappearance of all the secondary peaks and, most unexpected, the disappearance of one of the primary peak Nu regions, the on above jet number 4. The relevant computations, Figure 4d), exhibit the first two effects of rotation on the thermal characteristics, but none of the five primary regions of peak Nusselt number is predicted to disappear, or even to diminish relative to the others. The present computations, consequently, fail to reproduce the most important effect of rotation on leading edge impingement cooling.
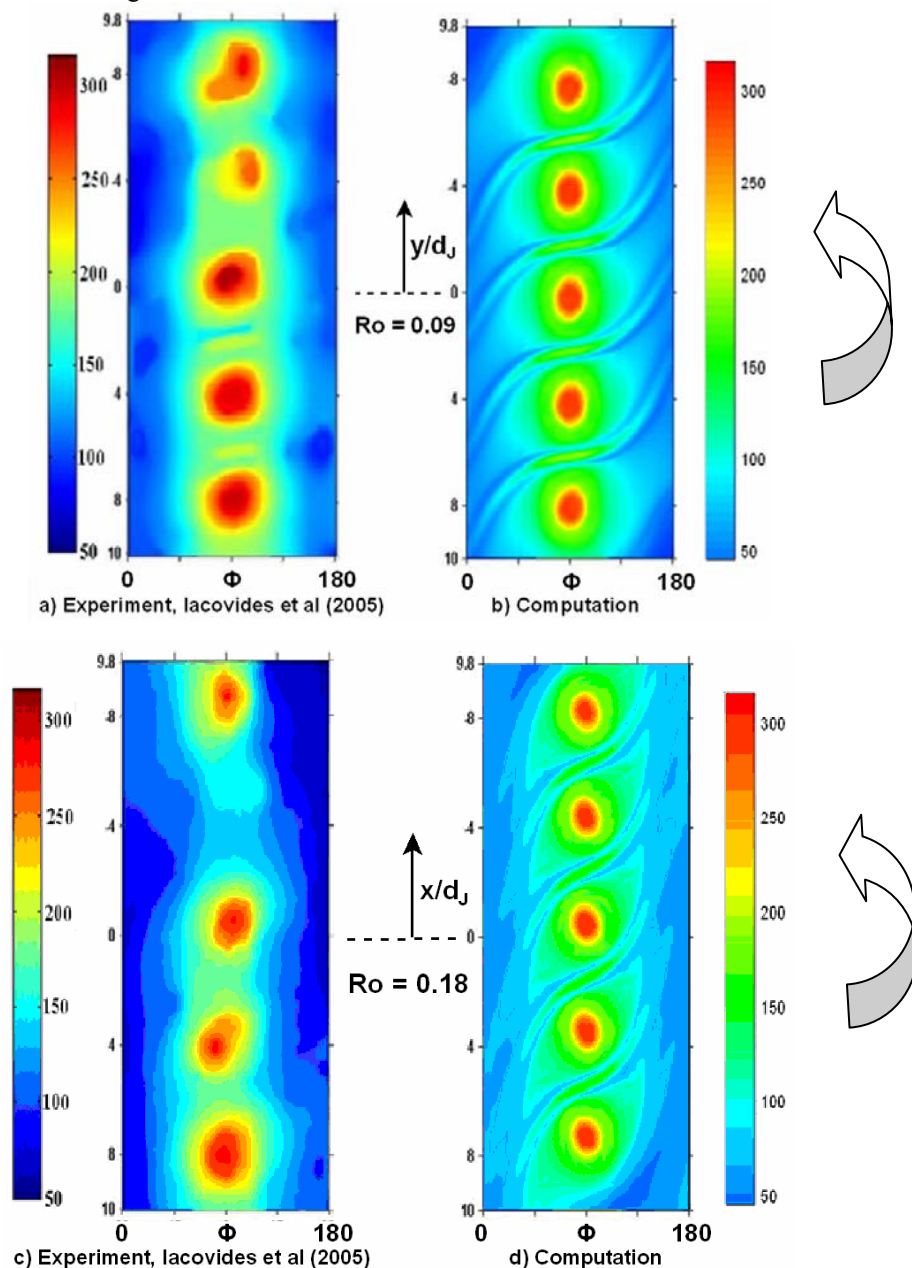

Figure 10. Nusselt number comparisons for rotating cases, Re=15,000 and Pr =6.09

As discussed by Iacovides et al (2005), the LDA and flow visualisation data, videos of the latter can be accessed at http://tmgflows.mace.manchester.ac.uk/, suggest that strong orthogonal rotation generates swirl within the jets, which in turn increases their spreading rate. The jets consequently overlap with each other before they reach the target surface. Due to the resulting flow instabilities, some jets, in this case jet 4, are prevented from reaching the target surface, which will explain the disappearance of the peak Nu region above this jet. The disappearance of the secondary peaks is also consistent with increase in the spreading rate of the jets. Moreover, Iacovides and Launder (2007) suggest that the rotation-induced swirl is generated in the chamber, upstream of the cooling passage and, due to the short injection holes, see Figure 1b), is transported into the cooling passage. The profile comparisons of the vertical velocity over the five jets under rotating conditions, shown in Figure 11, provide an opportunity to explore some of reasons why the computations fail to reproduce the experimental thermal behaviour. In comparison with the corresponding velocity profile for the stationary case at $y/d_J=1.34$, under stationary conditions, Figure 7, the centreline velocity of most jets is reduced by 20% and that of jet 4 by 60%. This is consistent with the experimentally observed increase in the spreading rate, along the x-y, stream-wise plane. In the computations, on the other hand, for all jets the centreline velocity at 1.34 diameters after the exit has the same value as in the stationary case. The computations consequently do not show the same increase in spreading rate under rotation as the measurements. The complex flow phenomena that result from the overlapping jets, such as the rapid disappearance of jet number 4, do not occur in the computations. The question of why the predictions do not reproduce this effect of orthogonal rotation on the jet development is a harder one to answer. The use of second-moment closures, which in contrast to effective-viscosity models are sensitive to rotation, may result in an increase in the jets' spreading rate. Alternatively, as suggested by Iacovides and Launder (2007), the cause of this predictive failure could be the fact that the flow domain considered is entirely within the cooling passage. If, as Iacovides and Launder (2007) suggest, swirl is generated as the cooling fluid enters the jet injection hole under rotating conditions, then it is not possible to impose the appropriate inlet conditions using the current domain that only covers the cooling passage itself. The domain will need to be extended to include the injection holes and also the chamber on the upstream side. Clearly further computations are needed to establish the cause of these predictive failures under rotating conditions and to suggest appropriate solution and modelling strategies

CONCLUDING REMARKS.

The commercial code FLUENT has been employed to simulate the flow and thermal development in a semi-cylindrical passage, in which the concave surface is cooled by a row of impinging jets, and which can rotate orthogonally, about an axis normal to the passage and parallel to the cooling jets. A structured multi-block
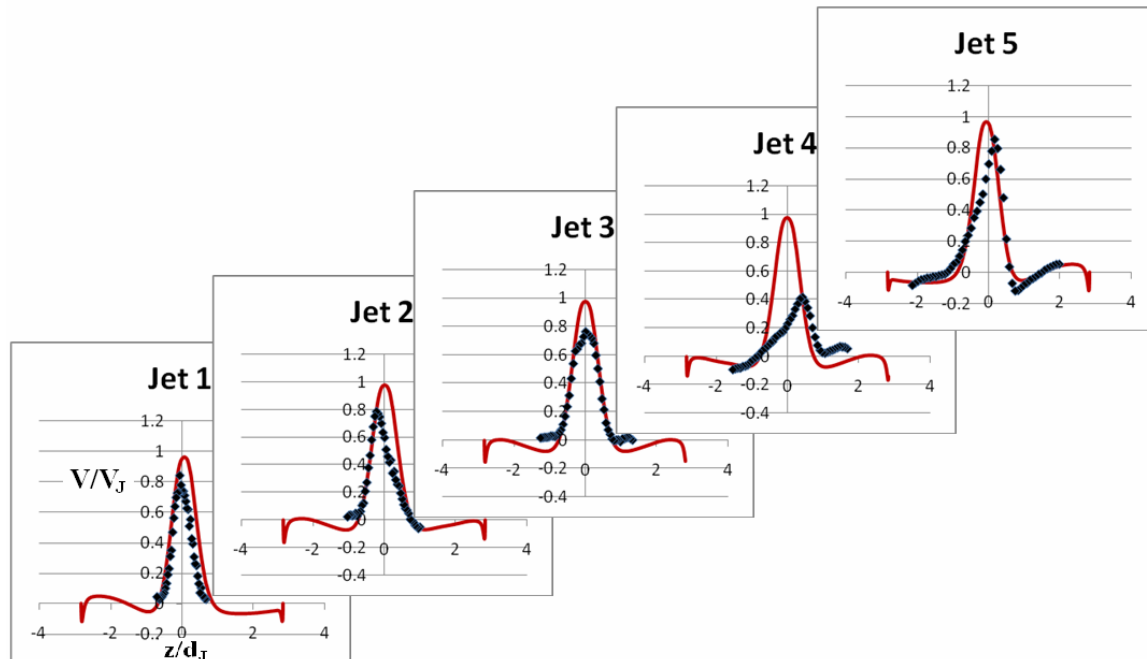

Figure 11. Comparisons of profiles of the vertical velocity component across the passage, at 1.34 jet diameters over each jet. Rotating case, Re= 9,400, Ro=0.18.

grid was generated, to reproduce the passage geometry, while at the same time providing adequate resolution of the new-wall regions. The realizable k-ε model has been employed, with the 2-layer "enhanced wall treatment", accounting for the effects of near-wall turbulence. It has been shown that with the chosen turbulence modelling strategy, nearly 2.5 million control volumes are necessary to adequately resolve the flow within the domain.

Under stationary conditions, the flow and thermal developments are reproduced faithfully enough to be adequate for industrial applications. Turbulence levels are under-estimated and, possibly as a result, the centreline velocity is under-estimated near the impingement surface. The levels and the distribution of the local Nusselt number are well predicted, with perhaps the under-estimation of the size of the peak Nu regions above each jet being the most significant deviation from the measured behaviour. It is argued that models that treat turbulence as non-isotropic and also a more refined approach to the modelling of near-wall turbulence are needed for further predictive improvements.

Under rotating conditions, there are further deviations between predictions and experimental data, to the extent that at the higher rotation rates, the most prominent feature of the thermal is not reproduced, most probably because the spreading rate of the jets is not predicted to increase with rotation. While the turbulence modelling issues identified in the previous paragraph in relation to the predictions in the stationary passage are also relevant, for the rotating conditions, the extension of the computational domain to include the flow within the injection holes and in the chamber upstream must also be explored.

NOMENCLATURE

d_J	jet diameter
k	turbulent kinetic energy or fluid thermal conductivity
L	length of semi-cylindrical passage
Nu	Nusselt number ($\equiv q_w.d_J/\{k(\Theta_W-\Theta_J)\}$)
P	fluid pressure
q_w	wall heat transfer per unit area
Pr	fluid Prandtl number
R	radius of semi-cylindrical passage
Ra	rotational Rayleigh number ($\equiv \Omega^2 X d_J^3 \sigma \beta \Delta\Theta/\nu^2$)
Re	jet flow Reynolds number ($\equiv V_j d_j/\nu$)
Ro	jet rotation number ($\equiv \Omega d_j/V_j$)
s	distance between centres of jet injection holes
U_j	mean Cartesian velocity component
u_i	fluctuating Cartesian velocity component
V_J	jet bulk velocity
X	distance from axis of rotation
X_i	Cartesian component of distance from centre of rotation
x	axial co-ordinate with the central jet as the origin
x_i	Cartesian tensor co-ordinate
Y	wall distance
y	vertical co-ordinate (parallel to the jet axis)
y^+	dimensionless wall distance [$\equiv Y(\tau_w/\rho)^{1/2}/\nu$]
z	cross-passage co-ordinate
α	fluid thermal diffusivity
β	coefficient of thermal expansion
$\Delta\Theta$	difference between wall and jet inlet temperature
ε	dissipation rate of turbulence
Θ	fluid mean temperature
Θ_J	jet inlet temperature
Θ_W	wall temperature
θ	fluid fluctuating temperature
μ	fluid dynamic viscosity
μ_t	turbulent dynamic viscosity
ν	fluid kinematic viscosity
ρ	fluid density
σ_Θ	turbulent Prandtl number
τ_w	wall shear stress
Ω	angular speed of rotation
Ω_i	Cartesian component of rotation tensor

REFERENCES

Akella K.V and Han J.C, "Impingement cooling in rotating two-pass rectangular channels.", AIAA Journal of Thermophysics and Heat Transfer, Vol 12, No 4, pp 582-588, 1998.

Craft T.J, Iacovides H, Mostafa N.A, "Modelling of Three-Dimensional Jet Impingement Cooling on a Concave Surface", 7th European Turbomachinery Conference, Athens, March 2007.

Han, J-C, Dutta, S. and Ekkad, S. "Gas-Turbine Heat Transfer and Cooling Technology", Taylor & Francis, 2000.

Iacovides H, Kounadis D, Launder B. E, Li J-K and Xu Z, "Effects of Rotation on the Flow and Thermal Development of a Row of Jets Impinging on a Concave Surface.", UK National Heat Transfer Conference, Oxford, 2003

Iacovides H, Kounadis D, Launder B. E, Li J-K and Xu Z, "Experimental Study of the Flow and Thermal Development of a Row of Cooling Jets Impinging on a Rotating Concave Surface.", ASME Journal of Turbomachinery, Vol 127, pp 222-229, 2005.

Iacovides H and Launder B E, "The computation of momentum and heat transport in turbulent flow around pipe bends.", 1st UK National Heat Transfer Conference, Leeds, 1984.

Iacovides H and Launder B E, "Turbulent momentum and heat transport in square-sectioned ducts rotating in orthogonal mode.", Numerical Heat Transfer, **12**, p 475, 1987.

Iacovides H and Launder B.E., "Internal blade cooling: the Cinderella of C&EFD research in gas turbines.", **Review Paper**, Proceedings of the I.Mech.E, Part A, Journal of Power and Energy, To Appear (2007)

Mattern, C., Hennecke, D. (1996), "The influence of rotation on impingement cooling", in ASME Paper 96-GT-161, Int. Gas Turbine and Aero Congress, Birmingham, UK.

Parsons J.A and Han H.C, "Rotation effect on jet impingement heat transfer in smooth rectangular channels with heated target walls and radially outward cross-flow.", International Journal of Heat and Mass Transfer, Vol 41, No 13, pp 2059-2071, 1998.

Son C, Gillespie D, Ireland P and Daley G.M, "Heat transfer and flow characteristics of an engine representative impingement cooling system.", ASME J. Of Turbomachinery, Vol 123, pp 153-160, 2001.

Wolfstein, **M.** "The Velocity and Temperature Distribution of One-Dimensional Flow with Turbulence Augmentation and Pressure Gradient" Vol. 12, 1969.